PROCEEDINGS OF SCIENCE

CMS results from PbPb collisions at the LHC

Igor Lokhtin* **(for the CMS Collaboration)**
D.V. Skobeltsyn Institute of Nuclear Physics, M.V. Lomonosov Moscow State University, Moscow, Russia
E-mail: Igor.Lokhtin@cern.ch

First results of the CMS experiment from PbPb collisions at nucleon-nucleon center of mass energy 2.76 TeV are presented. Thanks to its very large acceptance, fine granularity electromagnetic and hadronic calorimetry, superior muon and tracking systems, and powerful data acquisition and trigger systems, CMS is an excellent device for the study of hard probes of quark-gluon matter as well as global event properties in heavy-ion collisions at the LHC.

QFTHEP 2010
September 24 - October 1, 2011
Sochi, Russia

*Speaker.

PoS(QFTHEP2011)017

1. Introduction

The study of the fundamental theory of the strong interactions (Quantum Chromodynamics, QCD) in the regimes of extreme densities and temperatures is one of the primary goals of the modern high energy physics. The experimental and phenomenological study of multiple particle production in ultrarelativistic heavy-ion collisions is expected to provide valuable information on the (thermo)dynamical behavior of QCD matter in the form of a quark-gluon plasma (QGP), as predicted by lattice QCD calculations. The particular urgency of above topic is related to the begin of operation of the CERN Large Hadron Collider (LHC) with heavy-ion beams. The LHC currently delivers nucleus-nucleus collisions at the energy $\sqrt{s}_{\rm NN} = 2.76$ TeV, which is 14 times higher than those of RHIC. Three LHC experiments (ALICE, ATLAS and CMS) have collected the data on various physical observables during the 2010 PbPb run.

A detailed description of CMS program to carry out a series of PbPb measurements has been presented in the special addendum to CMS Physics Technical Design Report [1]. Heavy ion observables accessible to measurement with CMS include:

- "Soft" probes: global particle and energy rapidity densities, elliptic flow and spectra of low transverse momentum hadrons. These observables are mostly sensitive to the space-time evolution of the system once thermalization has set in and thus carry information about the thermodynamical properties of the produced QCD matter.

- "Hard" probes: jets, photons, quarkonia, Z-bosons and high-$p_{\rm T}$ hadrons, which are produced with high transverse momenta $p_{\rm T}$ or large masses M (much greater than the typical QCD scale of confinement: $p_{\rm T}$, $M \gg \Lambda_{\rm QCD} = 200$ MeV). The hard probe production cross sections can be described in the framework of perturbative QCD theory. Such hard particles are produced at the very early stages of the evolution of the system and thus are potentially affected by final-state interactions as they traverse the produced medium. Modifications with respect to the "vacuum QCD" spectra and cross-sections measured in proton-proton collisions, provide direct information on the dynamical and transport properties of the system: initial parton densities, transport coefficient of the medium, critical energy density.

In this contribution, the overview of first results of the CMS experiment obtained from PbPb collisions at $\sqrt{s}_{\rm NN} = 2.76$ TeV is presented. CMS recorded $\mathscr{L}_{\rm int} = 7.28\ \mu{\rm b}^{-1}$ of PbPb events in November 2010, and $\mathscr{L}_{\rm int} = 225\ {\rm nb}^{-1}$ of pp events at $\sqrt{s} = 2.76$ TeV in March 2011. For most hard probe studies the latter is used as a reference for the PbPb measurement.

2. CMS detector and its operating with lead beams

CMS is a general purpose experiment at the LHC designed to explore the physics at the TeV energy scale [2]. Since the CMS detector subsystems have been designed with a resolution and granularity adapted to cope with the extremely high luminosities expected in the proton-proton running mode, CMS can also deal with the large particle multiplicities anticipated for heavy-ion collisions. The central element of CMS is the magnet, a 13 m long, 6 m diameter, high-field solenoid (a uniform 3.8 T field) with an internal radius of ≈ 3 m. The tracker covers the pseudorapidity region $|\eta| < 2.5$ and is composed of two different types of detectors: silicon pixels and

silicon strips. The pixel detector consists of three barrel and two forward layers located close to the interaction region. Silicon strip detectors are divided into inner and outer sections and fill the tracker area with 10 layers in the transverse direction and 12 layers in longitudinal direction. The hadronic (HCAL) and electromagnetic (ECAL) calorimeters are located inside the coil (except the forward calorimeter, HF) and cover (including HF calorimeter) from -5.2 to 5.2 in pseudorapidity. The CMS muon stations cover the pseudorapidity region $|\eta| < 2.4$ and consist of drift tube chambers (DT) in the barrel region, $|\eta| < 1.2$, cathode strip chambers (CSCs) in the endcap regions, $0.9 < |\eta| < 2.4$, and resistive plate chambers (RPCs) in both barrel and endcaps, for $|\eta| < 2.1$. Note that CMS is the largest acceptance detector at the LHC with unique detection capabilities also in the very forward hemisphere with the CASTOR ($5.2 < \eta < 6.7$) and a pair of Zero-Degree calorimeters (ZDCs, $|\eta_{\rm neut}| > 8.3$).

The CMS trigger and data acquisition systems were specially configured for the 2010 PbPb run to prepare for the large multiplicities. In particular, the silicon micro strip tracker and the ECAL and HCAL calorimeters were read out in non-zero suppressed mode, recording the information from all channels. The zero suppression was done during the offline processing using algorithms optimized for PbPb environment. The maximum inelastic PbPb collision rate achieved during the run was about 220 Hz, while the maximum rate that could be written to tape was about 140 Hz. CMS employed its flexible triggering system to select and write to tape all events containing high-$p_{\rm T}$ jets, photons and muons while recording a scaled-down random sample of minimum bias events. For analysis of heavy ion events, it is important to determine the event centrality – overlap in the transverse plane (or impact parameter) of the two colliding nuclei. In CMS, centrality was determined using the total sum of transverse energy in reconstructed towers from HF calorimeters. For some studies the energy carried by neutral spectator fragments measured in the ZDC was used as a cross-check of centrality determination. Centrality for specific event classes is expressed as a percentage of the inelastic nucleus-nucleus interaction cross section.

3. Jets and photons

Studying the modification of jets as they are formed from high $p_{\rm T}$ partons propagating through the hot and dense QGP has been proposed as a particularly useful tool for probing the produced matter's properties. Jets were reconstructed in PbPb collisions at CMS using primarily the calorimeter information in a data sample corresponding to an integrated luminosity of $L_{\rm int} = 6.7\ \mu{\rm b}^{-1}$. Events having at least two jets with the leading (sub-leading) jet with transverse momentum $p_{\rm T}$ of at least 120 (50) GeV/c, pseudorapidity $|\eta| < 2$ and an opening angle $\Delta\varphi_{12} > 2\pi/3$ were selected to study these medium effects.

The most striking observation is the large, centrality-dependent, imbalance in the energy of the two jets, as measured in the CMS calorimeters [3]. To characterize the dijet momentum balance (or imbalance) quantitatively, the asymmetry ratio A_J is used,

$$A_{\rm J} = \frac{p_{\rm T,1} - p_{\rm T,2}}{p_{\rm T,1} + p_{\rm T,2}}\ , \tag{3.1}$$

where the subscript 1 always refers to the leading jet, so that $A_{\rm J}$ is positive by construction. The use of $A_{\rm J}$ removes uncertainties due to possible constant shifts of the jet energy scale.

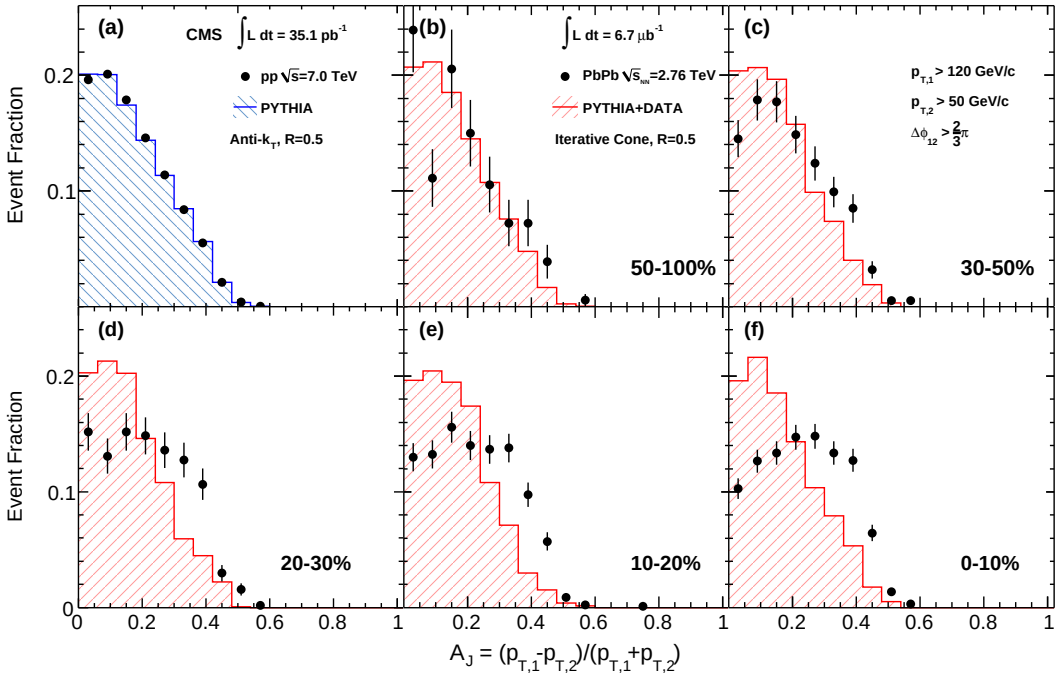

Figure 1: Dijet asymmetry ratio, A_J, for leading jets of $p_{T,1}$ >120 GeV/c, sub-leading jets of $p_{T,2}$ >50 GeV/c, and $\Delta\phi_{12} > 2\pi/3$ for 7 TeV pp collisions (a) and 2.76 TeV PbPb collisions in several centrality bins: (b) 50–100%, (c) 30–50%, (d) 20–30%, (e) 10–20% and (f) 0–10%. Data are shown as black points, while the histograms show (a) PYTHIA events and (b)-(f) PYTHIA events embedded into PbPb data. The error bars show the statistical uncertainities [3].

In Fig. 1 (a), the A_J dijet asymmetry is calculated with PYTHIA event generator and compared to pp data at $\sqrt{s} = 7$ TeV. The data and Monte-Carlo simulations are found to be in excellent agreement. This observation, as well as the good agreement between PYTHIA events embedded into PbPb data and the most peripheral PbPb data shown in Fig. 1 (b), suggests that PYTHIA at $\sqrt{s} = 2.76$ TeV can serve as a good reference for the dijet imbalance analysis in PbPb collisions. The centrality dependence of A_J for PbPb collisions can be seen in Figs. 1 (b)-(f), in comparison to PYTHIA simulations embedded into PbPb data. The dijet momentum balance exhibits a dramatic change in shape for the most central collisions. In contrast, the PYTHIA simulations only exhibit a modest broadening, even when embedded in the highest multiplicity PbPb events. At the same time, the detector-level leading jet spectra in PbPb data and the corresponding results for PYTHIA events embedded into PbPb samples show good quantitative agreement in all centrality bins over the p_T range studied. It confirms that the considered dijet configurations are presumably dominated by a "surface emission", when the dijet production vertex is close to the surface of the nuclear overlapping area. In this case one partonic jet escapes from the dense zone almost without interactions producing the leading hadronic jet, while a second partonic jet is affected by medium-induced multiple interactions producing the "quenched" sub-leading hadronic jet. Strong increase in the fraction of highly unbalanced jets in central PbPb collisions compared with peripheral collisions and model calculations, is consistent with a high degree of jet quenching in the produced

matter.

To find the lost ("missing") sub-leading jet energy, the calorimetric measurement was complemented by a detailed study of low p_{T} charged particles in the tracker and by using missing p_{T} techniques. The calorimeter-based momentum imbalance is reflected in the associated track distributions, which show a softening and widening of the sub-leading jet fragmentation pattern for increasing dijet asymmetry, while the high-p_{T} components of the leading jet remain nearly unchanged. Studies of the missing transverse momentum projected on the jet axis have shown that the overall momentum balance can be recovered if tracks at low p_{T} are included. In the PbPb data, but not in the simulations, a large fraction of the balancing momentum is carried by tracks having $p_{\mathrm{T}} < 2$ GeV/c. Comparing the momentum balance inside and outside of cones of $\Delta R = 0.8$ around the leading and sub-leading jet axes demonstrates that a large contribution to the momentum balance in data arises from soft particles radiated at $\Delta R > 0.8$ to the jets, a feature which is also not reproduced in PYTHIA simulations. Thus the apparent missing energy was found among the low p_{T} particles emitted outside of the sub-leading jet cone.

To further study jet properties in the PbPb environment, the hard component of jet fragmentation function was compared to the fragmentation of jets produced in pp collisions at the same energy. The comparison of fragmentation functions for PbPb and pp events for different centralities shows, that the distribution of charged particle momenta within the jet, normalized to the measured jet energy, looks strikingly the same (within uncertainties) to that seen in the equivalent jet energy produced in pp events [4].

As opposite to the case of strongly interacting partonic jets, high transverse energy prompt photons are not expected to be modified by the medium. Hence they provide direct test of perturbative QCD and the information to constrain the nuclear parton distribution functions. However, the measurement of prompt photons is complicated by the large background coming from the electromagnetic decays of neutral mesons produced in the fragmentation of other hard scattered partons. One can suppresses a large fraction of these decay photon background by imposing isolation cuts on the reconstructed photon candidates. CMS has shown photon purity measurement capabilities in pp collisions using the shower shape templates. In PbPb collisions at CMS, this technique was applied for the first time in heavy ion collisions to measure E_{T}-spectra of isolated photons with E_{T} from 20 GeV to 80 GeV in pseudorapidity range $|\eta| < 1.44$ [5]. A measurement of direct photon production as a function of event centrality and E_{T} was compared to the next-to-leading order (NLO) perturbative QCD calculations. To characterize the medium effects for hard probes, the nuclear modification factor R_{AA} is usually used. For prompt photons $R_{\mathrm{AA}} = dN^{\gamma}/(T_{\mathrm{AA}} \times \sigma^{\gamma}_{\mathrm{pp}})$, is computed from the PbPb measured yield dN^{γ}, the nuclear overlap function T_{AA} and the inclusive isolated photon cross-section $\sigma^{\gamma}_{\mathrm{pp}}$ given by the NLO pQCD calculation. The nuclear overlap function T_{AA} is equal to the number of elementary nucleon-nucleon binary collisions divided by the elementary NN cross section, and can be interpreted as the NN equivalent integrated luminosity per AA collision, at a given centrality. Figure 2 shows the R_{AA} as a function of PbPb centrality (defined here through the number of participating nucleons, N_{part}) for different E_{T} bins. Within statistical uncertainties, no modification for direct photon spectra is observed in PbPb collisions for all centralities with respect to the model calculations scaled by the number of incoherent nucleon-nucleon collisions. This establishes the prompt photons as unmodified hard probes in the studies of the produced medium in heavy ion collisions at the LHC.

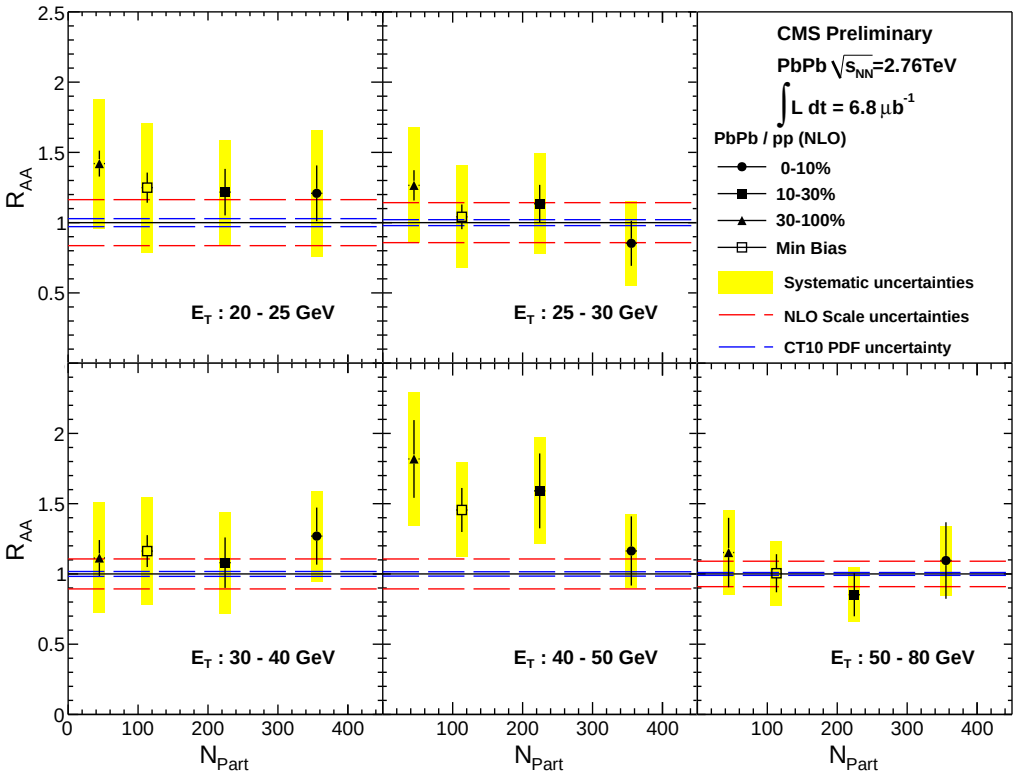

Figure 2: Nuclear modification factor R_{AA} as a function of N_{part} for the five different photon transverse energy intervals [5].

4. Quarkonia and Z-bosons

Quarkonia (the bound states of charm and bottom quarks) are important for studying QGP since they are predicted to be suppressed in heavy-ion collisions as compared to pp interactions. The magnitude of the suppression for different quarkonia states is expected to depend on their binding energy and on the medium temperature. By selecting events with opposite-sign dimuons, CMS measured production rates and momentum spectra of J/ψ-mesons and of the Υ family [6, 7].

Non-prompt J/ψ-mesons (those produced from B-meson decays) are identified at CMS by their displaced decay vertex. Thus the spectra of prompt and non-prompt charmonia were measured separately. The non-prompt J/ψ suppression is one measure of the medium-induced energy loss of b-quarks. Using data sets from PbPb and pp data at $\sqrt{s_{\mathrm{NN}}} = 2.76$ TeV, the quarkonium production measured in PbPb collisions is compared to expectations from an independent superposition of nucleon-nucleon collisions expressed in terms of the nuclear modification factor:

$$R_{\mathrm{AA}} = \frac{\mathscr{L}_{\mathrm{pp}}}{T_{\mathrm{AA}} N_{\mathrm{MB}}} \frac{N_{\mathrm{PbPb}}(\mathrm{Q\bar{Q}})}{N_{\mathrm{pp}}(\mathrm{Q\bar{Q}})} \cdot \frac{\varepsilon_{\mathrm{pp}}}{\varepsilon_{\mathrm{PbPb}}}. \tag{4.1}$$

Here T_{AA} is the nuclear overlap function, $\mathscr{L}_{\mathrm{pp}}$ is the pp luminosity, N_{MB} is the measured number of equivalent minimum bias PbPb events, $\frac{N_{\mathrm{PbPb}}(\mathrm{Q\bar{Q}})}{N_{\mathrm{pp}}(\mathrm{Q\bar{Q}})}$ is the raw yield ratio, and $\frac{\varepsilon_{\mathrm{pp}}}{\varepsilon_{\mathrm{PbPb}}}$ is the multiplicity dependent fraction of the efficiency ($\frac{\varepsilon_{\mathrm{pp}}}{\varepsilon_{\mathrm{PbPb}}} \sim 1.17$ for the most central bin).

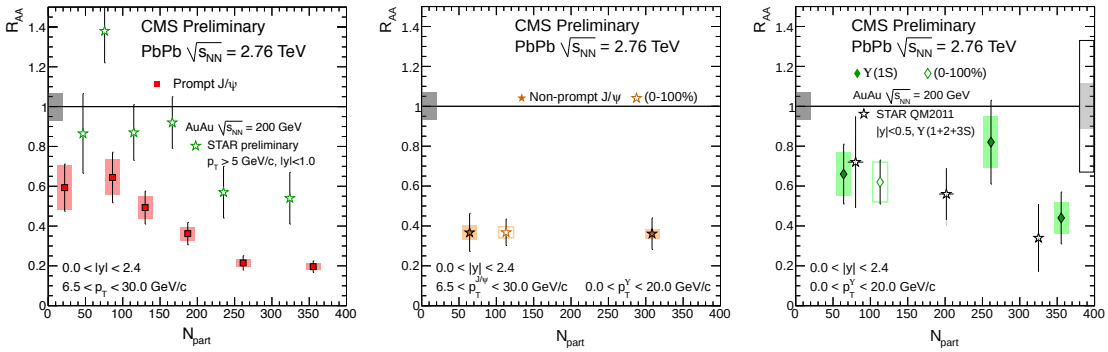

Figure 3: Nuclear modification factor $R_{\rm AA}$ as a function of $N_{\rm part}$ for prompt J/ψ (left), non-prompt J/ψ (center) and Υ (right). CMS data for prompt J/ψ and Υ are compared with the STAR data at RHIC [6].

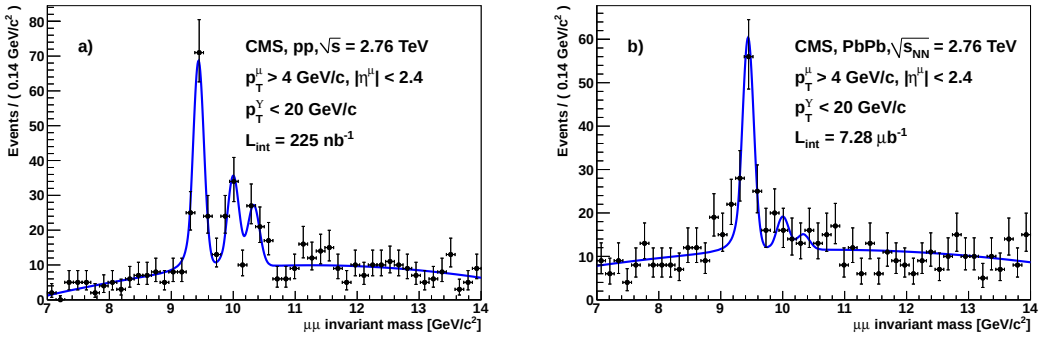

Figure 4: Dimuon invariant mass distribution in pp (left) and PbPb (right) collisions at $\sqrt{s_{\rm NN}} = 2.76$ TeV. The same reconstruction algorithm and analysis criteria are applied to both data sets. The solid lines show the result of the extended maximum likelihood fit [7].

Figure 3 shows the R_{AA} as a function of PbPb centrality ($N_{\rm part}$) for prompt J/ψ, non-prompt J/ψ and Υ [6]. A strong suppression of prompt J/ψ with $p_{\rm T} > 6.5$ GeV/c is measured in central collisions, and already in peripheral collisions, showing a clear dependence with centrality. In the 10% most central collisions, CMS observes a factor five suppression greater than measured by STAR experiment at RHIC. Non-prompt J/ψ, though strongly suppressed, show no strong centrality dependence within uncertainties. This is the first hint of b-quark energy loss in the hot medium. Furthermore, $\Upsilon(1S)$ are suppressed by about 40% in minimum bias collisions. It is showing a suppression of the same order of magnitude as measured at RHIC but with large uncertainty. Since a large fraction of the $\Upsilon(1S)$ yield arises from decays of heavier bottomonium states, this $\Upsilon(1S)$ suppression could be indirectly caused by the suppression of the excited states.

The excellent momentum resolution of the CMS detector results in well-resolved $\Upsilon(1S)$, $\Upsilon(2S)$ and $\Upsilon(3S)$ peaks in the dimuon mass spectrum in pp as well as in PbPb collisions (figure 4). Within the 7–14 GeV/c^2 mass range, there are 561 (628) opposite-sign muon pairs in the pp (PbPb) data set ($p_{\rm T}^{\mu} > 4$ GeV/c and $|\eta^{\mu}| < 2.4$). The ratio of $\Upsilon(2S+3S)/\Upsilon(1S)$ in PbPb and pp collisions benefits from an almost complete cancellation of possible acceptance and/or efficiency differences among

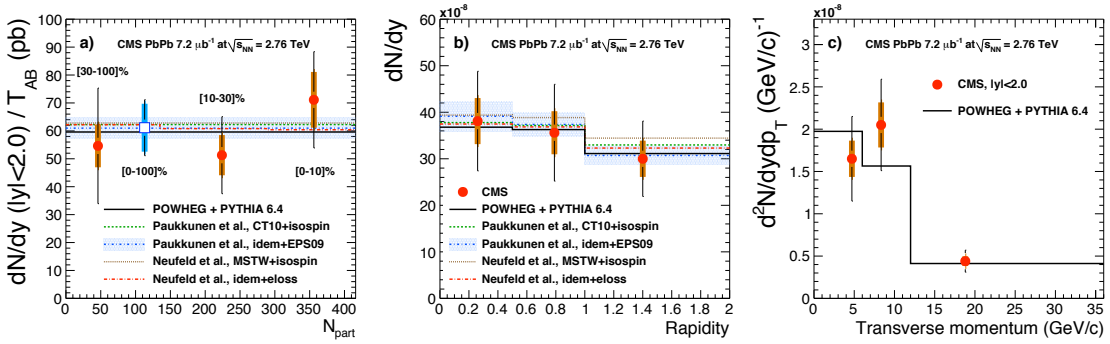

Figure 5: The yields of $Z \to \mu\mu$ per event: a) dN/dy divided by the nuclear overlap function $T_{\rm AB}$ as a function of $N_{\rm part}$, b) dN/dy versus the Z-boson rapidity y, c) $d^2N/dydp_{\rm T}$ versus the Z-boson transverse momentum $p_{\rm T}$. Data points are located horizontally at average values measured within a given bin. Vertical lines (bands) correspond to statistical (systematic) uncertainties [8].

the reconstructed resonances. The double ratio obtained is

$$\frac{\Upsilon(2S+3S)/\Upsilon(1S)|_{\rm PbPb}}{\Upsilon(2S+3S)/\Upsilon(1S)|_{\rm pp}} = 0.31^{+0.19}_{-0.15}\ (\text{stat.}) \pm 0.03\ (\text{syst.}), \tag{4.2}$$

where the systematic uncertainty arises from varying the line shape in the simultaneous fit, thus taking into account partial cancellations of systematic effects.The probability to obtain the measured value, or lower, if the true double ratio is unity, has been calculated to be less than 1%. This is consistent with differential melting of quarkonia states in the high temperatures produced by PbPb collisions, when $\Upsilon(1S)$ suppression is due to the melting of the excited states only.

The high energy collisions produced at the LHC allowed for the very first time to observe weak bosons, Z and W, in heavy-ion collisions. These weak bosons (like prompt photons) are not expected to interact with the strongly interacting medium and, as such, they provide a good test of perturbative QCD and the initial state nuclear effects. Z decays into pairs of both muons and electrons, as well as decays of W to a muon and a neutrino, were observed by CMS. In particular, the Z-boson yield in PbPb collisions at $\sqrt{s_{\rm NN}} = 2.76$ TeV has been measured inclusively and as a function of rapidity, transverse momentum, and event centrality [8]. The number of opposite-sign muon pairs observed in the 60–120 GeV/c^2 invariant mass range is 39, corresponding to a yield per unit of rapidity (y) and per minimum bias event of $(33.8 \pm 5.5(\text{stat}) \pm 4.4(\text{syst})) \times 10^{-8}$, in the $|y| <$ 2.0 range. The data was compared to the NLO perturbative QCD calculations, scaled by the number of elementary nucleon-nucleon collisions (figure 5). Within statistical and systematic uncertainties, no modification is observed with respect to the theoretical calculations. This measurement confirms the validity of the Glauber scaling for perturbative cross sections in nucleus-nucleus collisions at the LHC, and establishes the feasibility of carrying out detailed Z physics studies in heavy-ion collisions with the CMS detector. With PbPb collisions at higher luminosity, the Z boson promises to be a powerful reference tool for final-state heavy-ion related signatures as well as providing a means to study the modifications of the parton distribution functions.

5. Multiplicity and spectra

The multiplicity of charged particles produced in the mid-rapidity region is a key global observable to characterize the bulk properties of the matter created in heavy-ion collisions. The multiplicity density $dN_{\rm ch}/d\eta$ of primary charged hadrons in PbPb collisions was measured with CMS in runs without magnetic field in order to include particles with transverse momenta down to about 30 MeV/c [9]. The number of primary charged hadrons $N_{\rm ch}$ was defined as all charged hadrons produced in an event including decay products of particles with proper lifetimes less than 1 cm/c. The two methods based on the inner silicon pixel system was used. One technique involved counting the number of reconstructed single particle hits in the pixel detector, while the other formed hit pairs ("tracklets") from the different detector layers. It has been found that the two methods give consistent results (their average difference is smaller than 1%). Figure 6 shows the multiplicity density $dN_{\rm ch}/d\eta$ in mid-rapidity as a function of event centrality ($N_{\rm part}$) and $(dN_{\rm ch}/d\eta)/(N_{\rm part}/2)$ distributions as a function of η in various centrality bins. For the 5% most-central collisions, a primary charged hadron density of 1612 ± 55 is measured by CMS, which represents an increase of a factor of 3 compared to similar measurements at RHIC energies. The $dN_{\rm ch}/d\eta$ distributions, measured over the range $|\eta| < 2.5$, show weak η dependence (the variation being less than 10%). It was found [9] that the collision-energy dependence of the measured hadron multiplicities at central rapidities is well modelled by a power-law function of the type $a + s_{\rm NN}^n$.

Another important global observable that is sensitive to the energy density achieved in heavy ion collisions is the transverse energy E_T. Together with multiplicity measurement it gives information of how the initial energy is converted into particle production. The broad array of CMS calorimeters was used to measure $dE_{\rm T}/d\eta$ over a wide range of η [10]. This transverse energy density for the most central PbPb collisions is over 2 TeV per unit pseudorapidity at $\eta = 0$, which is about three times higher than at RHIC.

Together with jet measurements, the modification of charged particle $p_{\rm T}$-spectrum compared to nucleon-nucleon collisions at the same energy carries the information on the mechanisms of by which hard partons lose energy traversing the medium. The $p_{\rm T}$-spectrum and nuclear modification factor $R_{\rm AA}(p_{\rm T})$ were measured by CMS for all charged particles with $p_{\rm T}$ up to 100 GeV/c [11]. This factor was constructed according to the standard way,

$$R_{\rm AA}(p_{\rm T}) = \frac{d^2N^{\rm AA}/dp_{\rm T}d\eta}{T_{\rm AA}d^2\sigma^{\rm NN}/dp_{\rm T}d\eta}, \tag{5.1}$$

where $N^{\rm AA}$ and $\sigma^{\rm NN}$ represent the yield of charged particles in nucleus-nucleus collisions and the cross section in nucleon-nucleon collisions, respectively. For this analysis, pp reference was derived from an interpolation that includes CDF and CMS measurements at $\sqrt{s}$ =0.63–7 TeV [11]. The $R_{\rm AA}$ factor is presented as a function of transverse momentum in Fig. 7 for the six PbPb centrality bins. In the most peripheral events (70–90%), a moderate suppression by a factor of 2 ($R_{\rm AA} = 0.5$) is observed at low $p_{\rm T}$ with $R_{\rm AA}$ rising gently with increasing $p_{\rm T}$. The suppression is more pronounced in central collisions, as expected from the longer average path lengths traversed by hard-scattered partons as they lose energy in a hot matter. $R_{\rm AA}$ reaches a minimum value of 0.13 around 6–7 GeV/c in the 0–5% centrality. At higher $p_{\rm T}$, the value of $R_{\rm AA}$ rises and levels of above 40 GeV/c at a value of approximately 0.5. A rising $R_{\rm AA}$ at high $p_{\rm T}$ may reflect rather weak

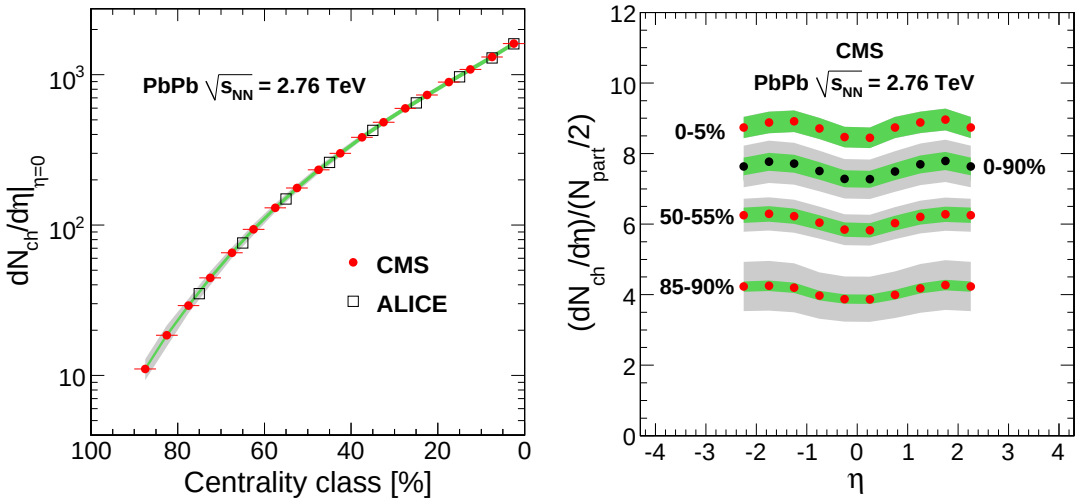

Figure 6: $dN_{\rm ch}/d\eta|_{\eta=0}$ as a function of PbPb centrality (left) and $dN_{\rm ch}/d\eta/(N_{\rm part}/2)$ distributions as a function of η in various centrality bins (right). For the left plot CMS data (solid circles) are compared with the ALICE (open squares). The inner green band shows the measurement uncertainties affecting the scale of the measured distribution, while the outer gray band shows the full systematic uncertainty [9].

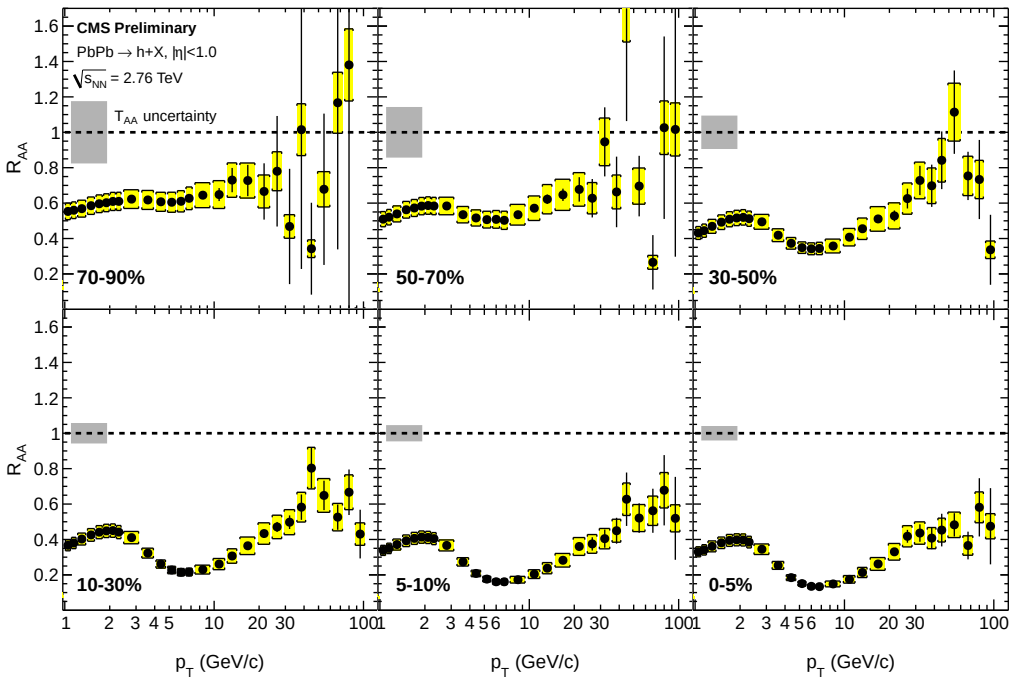

Figure 7: Nuclear modification factor $R_{\rm AA}$ (filled circles) as a function of $p_{\rm T}$ for six centrality intervals. The error bars represent the statistical uncertainties, and the yellow boxes – the $p_{\rm T}$-dependent systematic uncertainties. An additional systematic uncertainty from the normalization of nuclear overlap function $T_{\rm AA}$, common to all points, is shown as the shaded band around unity in each plot [11].

energy dependence of medium-induced partonic energy loss. It was shown [11] that the result is consistent with the values of $R_{\rm AA}$ measured by the ALICE within experimental uncertainties.

6. Long-range azimuthal correlations

Measurements of dihadron azimuthal correlations provide a powerful tool to study the properties of the strongly interacting medium created in ultrarelativistic nuclear collisions. At RHIC, dihadron azimuthal correlation measurements extending to large relative pseudorapidities resulted in the discovery of a ridge-shaped correlation in central AuAu collisions between particles with small relative azimuthal angles ($|\Delta\phi| \approx 0$), out to very large relative pseudorapidities ($|\Delta\eta|$). A striking ridge structure has also been observed in very high multiplicity proton-proton collisions $\sqrt{s} = 7$ TeV at the LHC by the CMS Collaboration [12], posing new challenges to the understanding of these long-range correlations. Moving onto PbPb collisions, dihadron correlations have been systematically studied at CMS as a function of centrality and particle transverse momentum [13, 14]. An example of the two-dimensional correlations for trigger particles with $4 < p_{\rm T}^{\rm trig} < 6$ GeV/c and associated particles with $2 < p_{\rm T}^{\rm assos} < 4$ GeV/c is shown in Fig. 8, starting from 0-5% corresponding to the most central collisions in the upper left-hand corner, to the 70-80% bin corresponding to the most peripheral ones in the lower right-hand corner. In the 0–5% most central PbPb collisions, a clear and significant ridge-like structure is observed at $\Delta\phi \approx 0$, which extends all the way to the limit of the measurement of $|\Delta\eta| = 4$. For more peripheral collisions, a $\cos(2\Delta\phi)$ component becomes prominent, which is attributed to the elliptic flow effect. It has been found [13] that the observed long-range ridge-like structure is most evident in the intermediate transverse momentum range, $4 < p_{\rm T}^{\rm trig} < 6$ GeV/c, and decreases to almost zero for $p_{\rm T}^{\rm trig}$ above 10–12 GeV/c. In addition, a Fourier decomposition of the one-dimensional $\Delta\phi$-projected correlation functions in the ridge region ($2 < |\Delta\eta| < 4$) was analyzed [14]. Higher order flow harmonics have been extracted as a function of centrality and transverse momentum, providing essential insights to the viscosity and initial condition of the PbPb collision system. The very broad solid-angle coverage of the CMS detector and the statistical accuracy of the sample analyzed provide significantly improved observations of short- and long-range particle correlations over previously available measurements.

7. Elliptic flow

In non-central heavy ion collisions, the initial spatial asymmetry of the collision zone leads to anisotropies in the final state charged hadron emission. This collective behavior is known as "flow" and is the result of the hydrodynamic expansion of the matter produced in the collision zone and is driven by pressure gradients. The strength of this flow is measured through a Fourier expansion of the charged hadron azimuthal distributions with respect to the reaction plane, defined by the impact parameter vector and collision direction. In particular, the elliptic flow parameter, v_2, is defined as the second harmonic coefficient in the Fourier expansion of the particle azimuthal distribution with respect to the reaction plane:

$$\frac{dN}{d\varphi} = \frac{N_0}{2\pi}[1 + 2v_1\cos(\varphi - \Psi_R) + 2v_2\cos 2(\varphi - \Psi_{\rm R}) + ...], \tag{7.1}$$

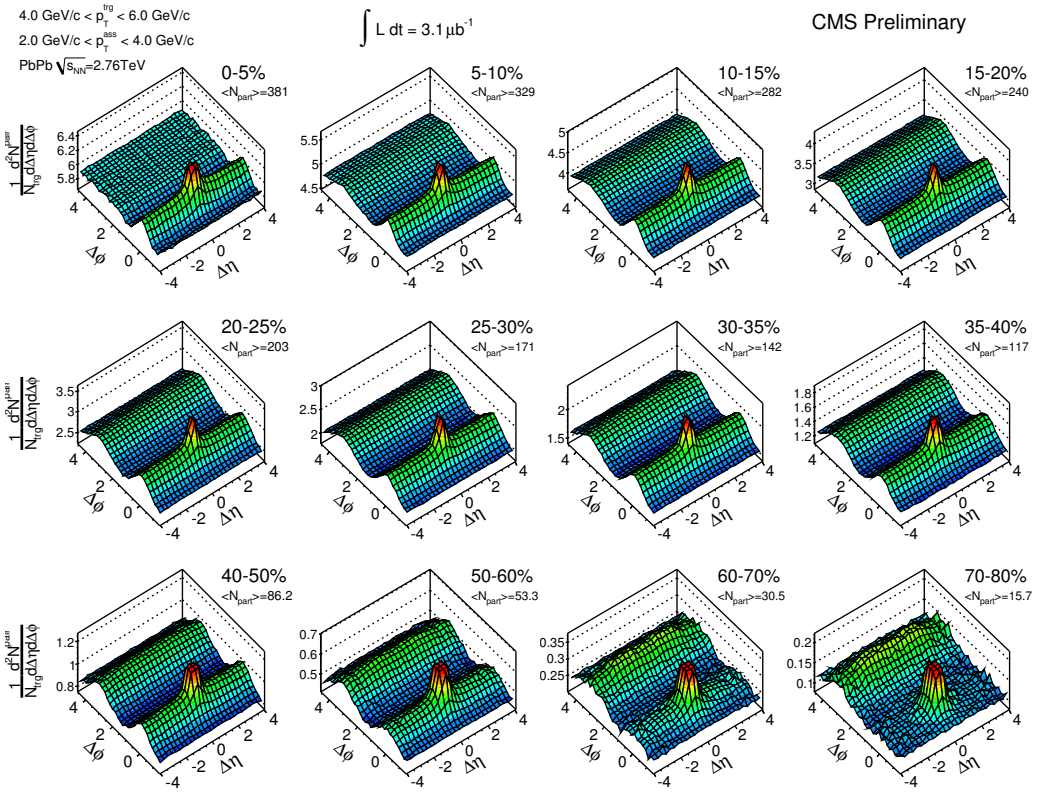

Figure 8: Two-dimensional per-trigger-particle associated yield of charged hadrons as a function of $\Delta\eta$ and $\Delta\phi$ for $4 < p_{\mathrm{T}}^{\mathrm{trig}} < 6$ GeV/c and $2 < p_{\mathrm{T}}^{\mathrm{assos}} < 4$ GeV/c in 12 centrality classes of PbPb collisions. The centrality labeling is such that 0-5% is the most central five percent of PbPb collisions [14].

where Ψ_{R} is the true reaction plane angle and N_0 stands for full multiplicity. Then v_2 is the average over particles of $\cos(2(\varphi - \Psi_{\mathrm{R}}))$. The higher-order coefficients of interest are v_3 (triangular flow), v_4 (quadrangular flow), v_5 (pentagonal flow), and v_6 (hexagonal flow).

The detailed measurements of the elliptic flow parameter and the higher harmonics (up to 6th order) as a function of centrality, transverse momentum and pseudorapidity were conducted at CMS [15, 16] using charged tracks reconstructed in the silicon tracker. The analysis was performed using 2.31 million PbPb events selected with a minimum bias trigger. The elliptic flow analysis was performed at CMS using several methods, including event plane, 2- and 4-particle cumulants and Lee-Yang Zeros (LYZ) [15]. Higher order flow analysis was performed with selected methods [16]. The odd harmonics, v_3 and v_5, were measured using the 2-particle cumulant method. Additionally, the fourth harmonic, v_4 was measured using the LYZ method and 3 and 5-particle cumulant methods, and the sixth harmonic, v_6 was measured using the LYZ method. For the event plane method, elliptic flow was measured with respect to event planes determined from tracks in the backward ($-2 < \eta < -1$) and forward ($1 < \eta < 2$) pseudorapidity regions. This provides a gap of $1 < \Delta\eta < 3.4$ between the tracks used in the elliptic flow measurement and those used in the event plane determination, which is expected to reduce the effect of non-flow correlations on the measurement. The cumulant method measures flow by a cumulant expansion of multi-particle

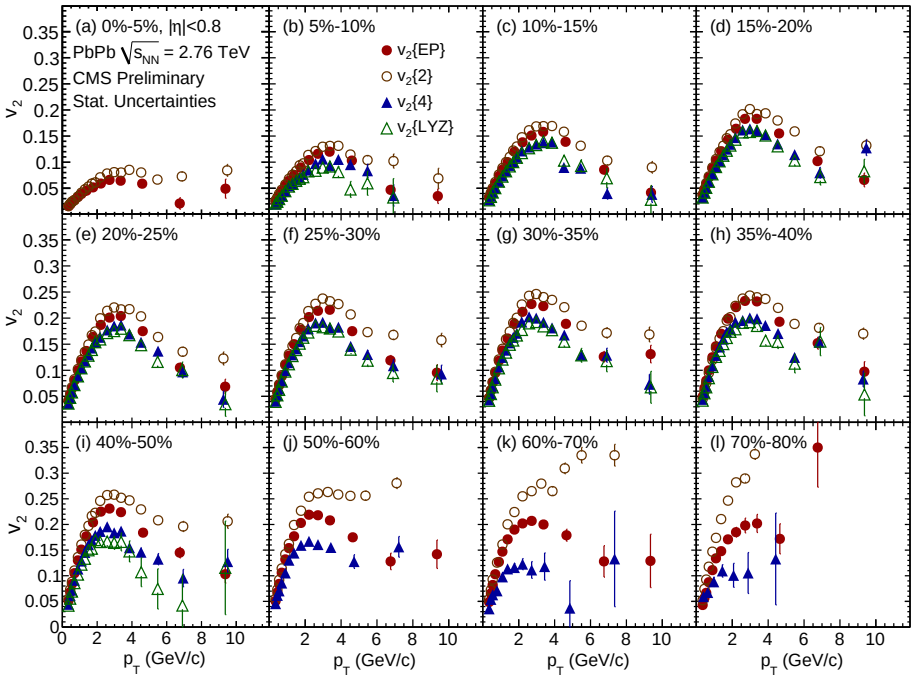

Figure 9: Elliptic flow coefficient v_2 obtained by different methods as a function of p_{T} at $|\eta| < 0.8$ for the 12 centrality classes. The error bars show the statistical uncertainties only [15].

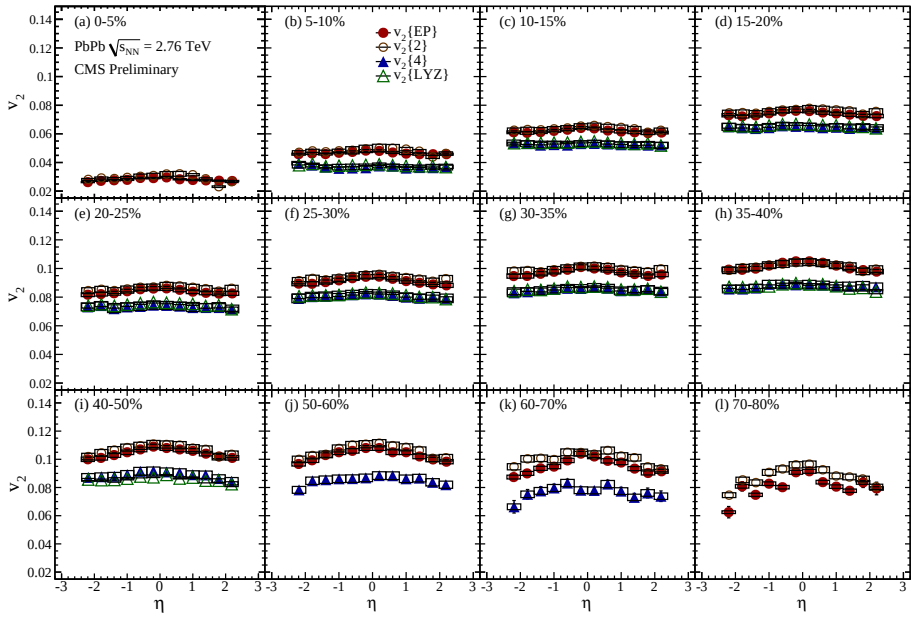

Figure 10: Elliptic flow coefficient v_2 obtained by different methods as a function of η at $0.3 < p_{\mathrm{T}} < 3.0$ GeV/c for the 12 centrality classes. The error bars show the statistical uncertainties, and boxes give the systematic uncertainties [15].

azimuthal correlations, and the flow harmonics are obtained from the cumulant terms of the expansion. The cumulant of the k-particle correlation, called the k^{th} order cumulant, removes the contribution of all lower order correlations and so is expected to remove the effect non-flow correlations between less than k particles. To calculate the cumulant expansion, a generating function of the multiparticle correlations in a complex plane was used. The LYZ method uses the large-order behavior of the cumulant expansion, rather than explicitly computing cumulants at a given order. The flow signal is obtained from the zeros in the complex plane of a generating function of azimuthal correlations.

Figures 9 and 10 show $p_{\mathrm{T}}-$ and $\eta-$dependencies of elliptic flow coefficient v_2 obtained with different methods for 12 centrality classes [15]. The four methods show differences consistent with their expected sensitivities to non-flow contributions. The method which is most affected by these is the 2-particle cumulant, while the 4th-order cumulant and the LYZ method being much less sensitive to such non-flow contributions. The value of v_2 increases from central to peripheral collisions as expected if the anisotropy is driven by the spatial anisotropy in the initial state. The transverse momentum dependence shows a rise of v_2 up to $p_{\mathrm{T}} \sim 3$ GeV/c and then a decrease (as expected due to the significant influence of jet component at high p_{T}). Only a weak η-dependence of v_2 is observed, except in the most peripheral events, which are more affected by non-flow correlations. The integrated v_n values at mid-rapidity as a function of event centrality was also measured [16]. It has been found that the flow effect is strongest for semi-peripheral events and in the second harmonic v_2. The higher order even harmonics, v_4 and v_6, show similar trends as v_2, although this is less pronounced in the case of v_6. The v_3 value is weakly dependent on centrality and remains sizable even for the most central collisions. These measurements may be used in conjunction with hydrodynamics calculations as a test of the theoretical models of the initial conditions.

8. Summary

Thanks to its very large acceptance, fine granularity electromagnetic and hadronic calorimetry, superior muon and tracking systems, and powerful data acquisition and trigger systems, CMS is an excellent device for the study of hard probes of quark-gluon matter as well as global event characteristics in heavy-ion collisions at the LHC. First CMS results from PbPb collisions at the energy $\sqrt{s}_{\mathrm{NN}} = 2.76$ TeV show a number of exiting collective features. The overall picture that emerges from the global event observables (multiplicity and spectra, long- and short-range dihadron azimuthal correlations, elliptic flow) is that strongly interacting matter with hydrodynamical properties has been created.

One of the most striking observations related to the hard probes is the large, centrality-dependent, imbalance in the energy of the two jets, as measured in the CMS calorimeters. Together with the strong suppression of inclusive high-p_{T} hadron yield, significant increase in the fraction of highly unbalanced jets in central PbPb collisions compared with peripheral collisions and model calculations, is consistent with a high degree of jet quenching in the produced matter. The complementary study with tracker using missing p_{T} techniques shows that the jet energy loss spreads over low p_{T} and large angles. At the same time, the distribution of charged particle momenta within the jet, normalized to the measured jet energy, looks the same in pp and PbPb collisions.

Another important observation is the suppression of different quarkonium states (J/ψ and Υ family) with varying binding energies. For the first time, the suppression of excited Υ states has been observed in heavy ion collisions, that is consistent with Debye screening of the colour charge in quark-gluon matter. The measured suppression of non-prompt $J/\psi-$meson yield may be the first hint of b-quark energy loss in the hot medium.

As opposite to the case of strongly interacting hard probes (such as jets, high-$p_{\rm T}$ charged hadrons and quarkonia), Z-bosons and prompt photons do not show any modification with respect to theoretical perturbative QCD calculations, scaled by the number of elementary nucleon-nucleon collisions. This establishes the electroweak hard probes as a powerful reference tool for final-state heavy-ion related signatures as well as providing a means to study the modifications of the parton distribution functions.

The scope and the level of detail of all CMS measurements validates the concept of using a general purpose, hermetic detector for studies of heavy-ion collisions. More differential analysis of above-mentioned effects, as well as some new measurements (γ+jet correlation, tagged B-jets), are expected from high luminosty PbPb collisions in 2011.

9. Acknowledgments

The author wishes to express the gratitude to the members of CMS Collaboration for fruitful cooperation. The author also gratefully acknowledge support from Dynasty Foundation.

References

[1] D. d'Enterria (ed.) et al. (CMS Collaboration), *J. Phys.* **G 34** (2007) 2307.

[2] S. Chatrchyan et al. (CMS Collaboration), *JINST* **3** (2008) S08004.

[3] S. Chatrchyan, et al. (CMS Collaboration), *Phys. Rev.* **C 84** (2011) 024906.

[4] S. Chatrchyan, et al. (CMS Collaboration), CMS PAS HIN-11-004.

[5] S. Chatrchyan, et al. (CMS Collaboration), CMS PAS HIN-11-002.

[6] S. Chatrchyan, et al. (CMS Collaboration), CMS PAS HIN-10-006

[7] S. Chatrchyan, et al. (CMS Collaboration), *Phys. Rev. Lett.* **107** (2011) 052302.

[8] S. Chatrchyan, et al. (CMS Collaboration), *Phys. Rev. Lett.* **106** (2011) 212301.

[9] S. Chatrchyan et al. (CMS Collaboration), *JHEP* **1108** (2011) 141.

[10] S. Chatrchyan, et al. (CMS Collaboration), CMS PAS HIN-11-003.

[11] S. Chatrchyan, et al. (CMS Collaboration), CMS PAS HIN-10-005.

[12] V. Khachatryan, et al. (CMS Collaboration), *JHEP* **09** (2010) 091.

[13] S. Chatrchyan et al. (CMS Collaboration), *JHEP* **1107** (2011) 076.

[14] S. Chatrchyan, et al. (CMS Collaboration), CMS PAS HIN-11-006.

[15] S. Chatrchyan, et al. (CMS Collaboration), CMS PAS HIN-10-002.

[16] S. Chatrchyan, et al. (CMS Collaboration), CMS PAS HIN-11-005.